Electronic Supplementary Material (ESI) for Physical Chemistry Chemical Physics.

Nitroxide-nitroxide and nitroxide-metal distance measurements in transition metal complexes with two or three paramagnetic centres give access to thermodynamic and kinetic stabilities

A. Giannoulis,[ab] K. Ackermann,[ab] P. E. Spindler,[c] C. Higgins,[b] D. B. Cordes,[b] A. M. Z. Slawin,[b] T. F. Prisner[c] and B. E. Bode*[ab]

[a]*Biomedical Sciences Research Complex and Centre of Magnetic Resonance University of St Andrews, North Haugh, St Andrews KY16 9ST*

[b]*EaStCHEM School of Chemistry, University of St Andrews, North Haugh, St Andrews KY16 9ST, UK*

[c]*Institute of Physical and Theoretical Chemistry and Center for Biomolecular Magnetic Resonance, Goethe-University Frankfurt am Main, Max-von-Laue-Str. 7, D-60438 Frankfurt am Main, Germany*

E-mail: beb2@st-andrews.ac.uk

Supporting information

Table of contents

1. General synthesis information page S2
2. Synthesis, characterization and nitroxide-nitroxide PELDOR of $Co^{II}\mathbf{L}_2(PF_6)_2$ page S3
3. Fe^{II} 'pseudo-titration' series page S6
4. Co^{II} 'pseudo-titration' series page S7
5. Cu^{II} 'pseudo-titration' series page S9
6. Modelled M^{II}-nitroxide modulation depths page S11
7. Details on WURST pulses page S11
8. Co^{II}-nitroxide distance measurements page S12
9. Cu^{II}-nitroxide distance measurements page S14
10. Synthesis and characterization of ligand **K** page S16
11. Scrambling/exchange mixtures page S20
12. References page S21

1. General synthesis information

Reactions using sensitive reagents were performed under an atmosphere of nitrogen with the use of dry solvents, with glass-ware flame dried and cooled under nitrogen. Dry DMF was purchased from Sigma-Aldrich and used as supplied. Triethylamine (NEt_3) for Sonogashira coupling reactions was freshly distilled from CaH_2, while all other solvents were used without further purification. Solvents used for Sonogashira coupling reactions were degassed by freeze-pump-thaw cycles (× 4). Petrol refers to petroleum ether 40-60 °C.

Room temperature (rt) refers to 20-25 °C; a temperature of 0 °C was achieved using an ice-water bath. Reflux conditions were achieved with the appropriate DrySyn heating block. The term *in vacuo* refers to the use of a rotary evaporator. Column chromatography was carried out either with silica gel 60 (Crawford Scientific) or with alumina, activated with 4% H_2O. Analytical thin layer chromatography was performed using pre-coated polystyrene thin layer chromatography (TLC) sheets or alumina TLC cards (Sigma-Aldrich). TLC visualization was achieved with ultraviolet irradiation, followed by staining in 1% aq. $KMnO_4$.

Melting points were recorded on an Electrothermal 9100 melting point apparatus and are uncorrected. Infrared spectra were acquired on a Shimadzu Fourier transform IR Affinity-1 infrared spectrometer. Mass spectrometric (*m*/*z*) data were acquired by atmospheric pressure chemical ionization (APCI) or nanospray ionization (NSI), at the EPSRC National Mass Spectrometry Service Centre, Swansea.

X-ray diffraction data for compound **1** and ligand **K** were collected at 173 K by using a Rigaku FR-X Ultrahigh Brilliance Microfocus RA generator/confocal optics with XtaLAB P200 diffractometer [Mo Kα radiation (λ = 0.71075 Å)]. Intensity data were collected using ω steps accumulating area detector images spanning at least a hemisphere of reciprocal space. All data were corrected for Lorentz polarization effects. A multiscan absorption correction was applied by using CrystalClear.[1] The structure of **1** was solved by Patterson methods (PATTY[2]), and that of **K** by direct methods (SIR2011[3]), while both structures were refined by full-matrix least-squares against F^2 (SHELXL-2014[4]). Non-hydrogen atoms were refined anisotropically, and hydrogen atoms were refined using a riding model. All calculations were performed using the CrystalStructure[5] interface. Selected crystallographic data are presented in Tables S1 and S2. CCDC 1497631 (**1**) and 1497632 (**K**) contain the supplementary crystallographic data for this paper. These data can be obtained free of charge from The Cambridge Crystallographic Data Centre via www.ccdc.cam.ac.uk/structures.

2. Synthesis, characterization and nitroxide-nitroxide PELDOR of $[Co^{II}L_2](PF_6)_2$

The formation of the bis-tpy Co^{II} complex with ligand **L** was tested by precipitating the complex with PF_6^- counter ions, *i.e.* as $[Co^{II}\mathbf{L}_2](PF_6)_2$ This was done by mixing 2.0 equiv. of **L** with 1.0 equiv. of $Co^{II}Cl_2$ forming the $[Co^{II}\mathbf{L}_2]Cl_2$ complex *in situ*. The title complex was isolated as dark brown powder after addition of excess NH_4PF_6 (Scheme S1).

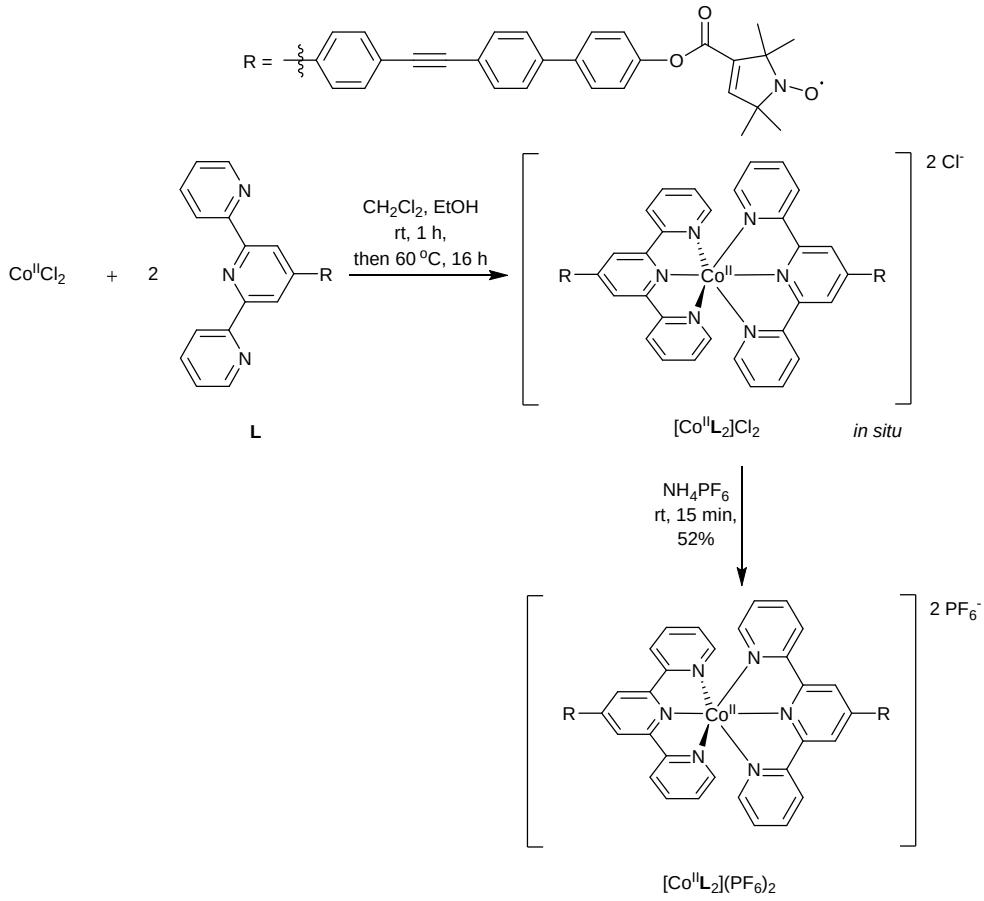

Scheme S1. Synthesis of $[Co^{II}L_2](PF_6)_2$.

A solution of $Co^{II}Cl_2$ (0.003 g, 0.023 mmol, 1.0 equiv.) in H_2O/MeOH 1/1 (10 mL) was added to a solution of **L** (0.03 g, 0.046 mmol, 2.0 equiv.) in CH_2Cl_2 (5 mL) and the mixture was heated to 60 °C for 16 h. Addition of further MeOH (7 mL) facilitated the miscibility of the ternary mixture. The reaction was left to cool to rt and was filtrated to remove the insolubles. An excess of NH_4PF_6 (0.05 g, 0.3 mmol, 13.0 equiv.) was added while stirring the filtrate and a brown precipitate formed immediately. The title complex was isolated by filtration (0.02 g, 0.012 mmol, 52%) as brown powder. mp 280.0-282.0 °C (dec.); ν_{max} (cm^{-1}) 790, 835, 1002, 1166, 1240, 1288, 1402, 1429, 1471, 1600, 1614, 1732; *m/z* (NSI^+) 696 ($[Co^{II}L_2]^{2+}$, 100%); HRMS (NSI^+) $C_{88}H_{70}CoN_8O_6$ ($[Co^{II}L_2]^{2+}$) found 696.7363, calculated 696.7370 (− 1.0 ppm); $C_{88}H_{70}CoN_8O_6P_2F_{12}$ calculated C, 62.75; H, 4.19; N, 6.65; found C, 62.60; H, 4.07; N, 6.58%.

The analytical data of complex $[Co^{II}\mathbf{L}_2](PF_6)_2$ are given in Fig. S1-S2 and the PELDOR distance measurement between the nitroxide spins in Fig. S3.

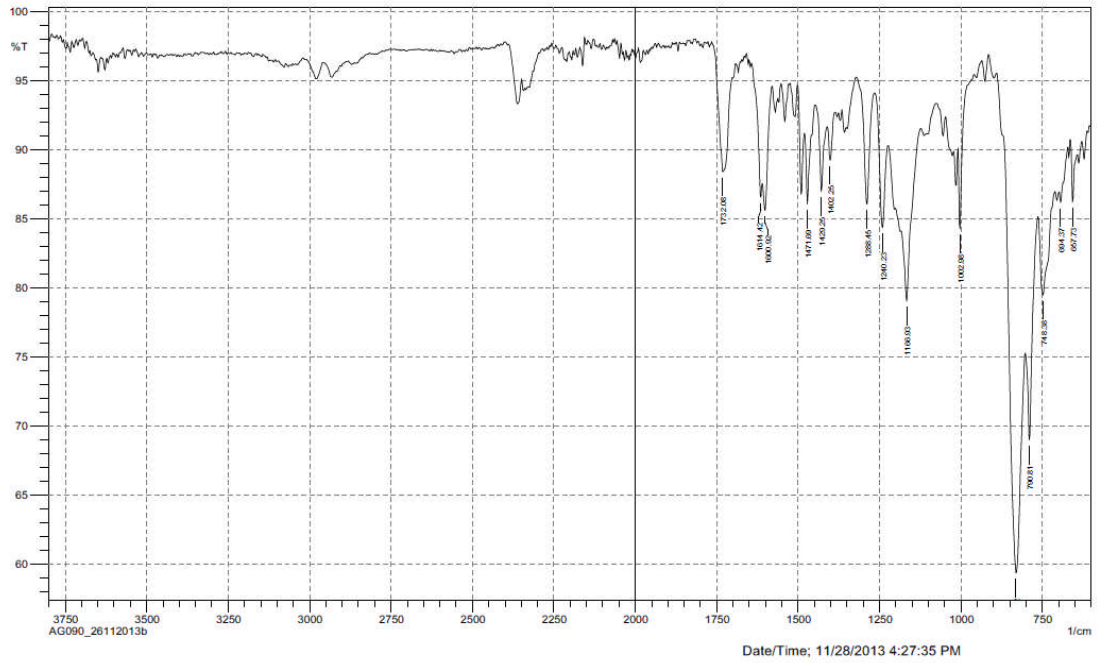

Fig. S1. IR spectrum of $[Co^{II}L_2](PF_6)_2$.

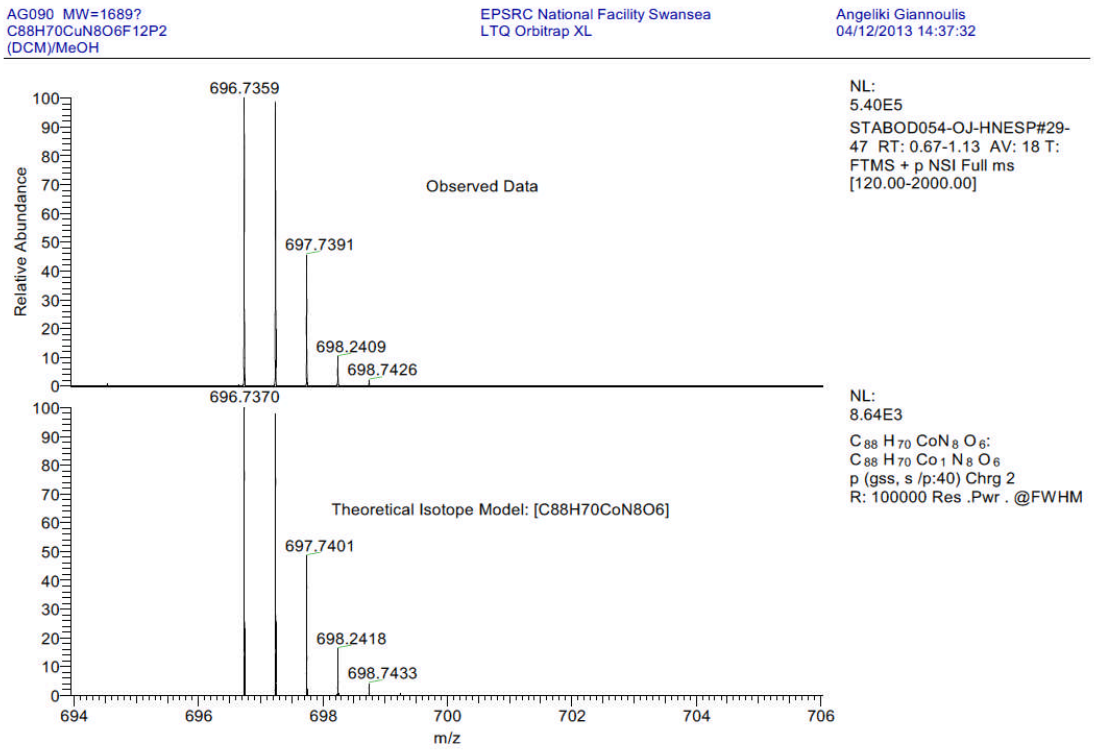

Fig. S2. Mass spectrum of $[Co^{II}L_2](PF_6)_2$.

We subjected $[Co^{II}\mathbf{L}_2](PF_6)_2$ to nitroxide-nitroxide PELDOR distance measurements, however poor solubility in most solvents and short phase memory times, T_m, did not allow measurements in reasonable amount of time (data not shown). We, therefore, *in situ* exchanged PF_6^- anions with BPh_4^- that gave improved solubility and improved relaxation properties of the nitroxide spins. PELDOR experiments were performed in a mixture of DMSO-*d*6/D_2O/ethylene glycol 8/1/1 at X-band frequencies at 10 K with final complex concentration of ~250 µM or ~500 µM in nitroxides (Fig. S3).

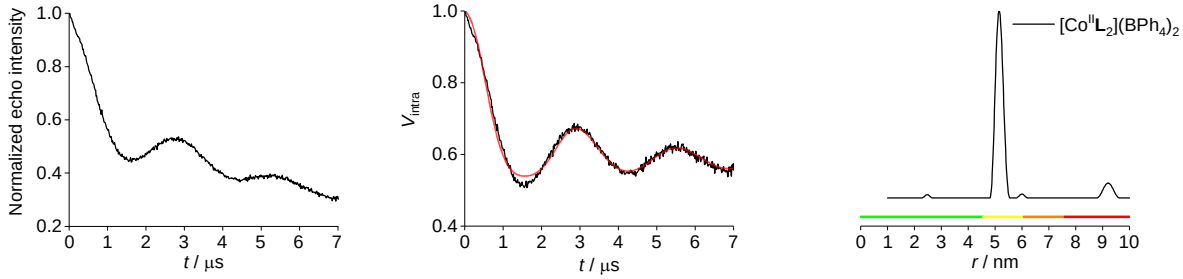

Fig. S3. Nitroxide-nitroxide PELDOR distance measurements at X-band frequencies at 10 K on $[Co^{II}L_2](BPh_4)_2$. Background uncorrected (left), background corrected (middle) PELDOR data and distance distribution (right).

3. Fe^{II} 'pseudo-titration' series

The nitroxide-nitroxide PELDOR measurements on the Fe^{II}/**L** series were performed at X-band frequencies at 50 K. The data are shown in Fig. S4.

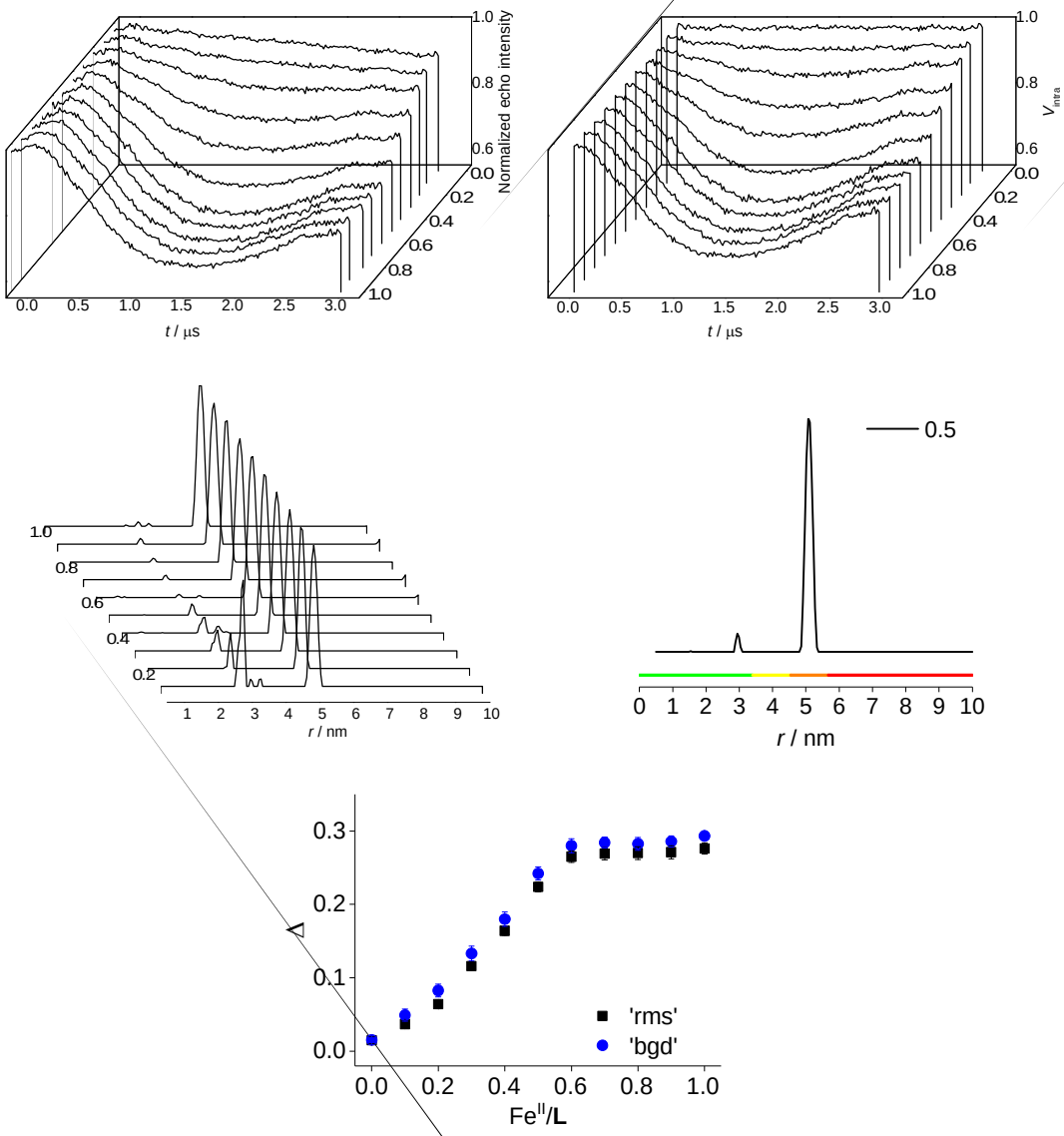

Fig. S4. Fe^{II} 'pseudo-titration' series measured with PELDOR at X-band. Background uncorrected (top left), background corrected (top right) PELDOR data, distance distributions (middle left) and distance distribution of the Fe^{II}/L = 0.5 ratio including colour coded reliability bars (middle right) and modulation depth Δ *vs* Fe^{II}/L as derived from the fit of the trace ('rms', black points, bottom) and upon variation of the background for densities between half and double that of the 0.0 ratio ('bgd', blue points, bottom).

4. Co^{II} 'pseudo-titration' series

In order to assess the optimum experimental temperature for performing PELDOR on the Co^{II} series, we measured the longitudinal and transverse relaxation times (T_1 and T_m, respectively) of the nitroxide spins as well as the modulation depth of the nitroxide-nitroxide PELDOR experiment over a range of temperatures of the Co^{II}/**L** = 0.5 complex at Q-band frequencies (Fig. S5)

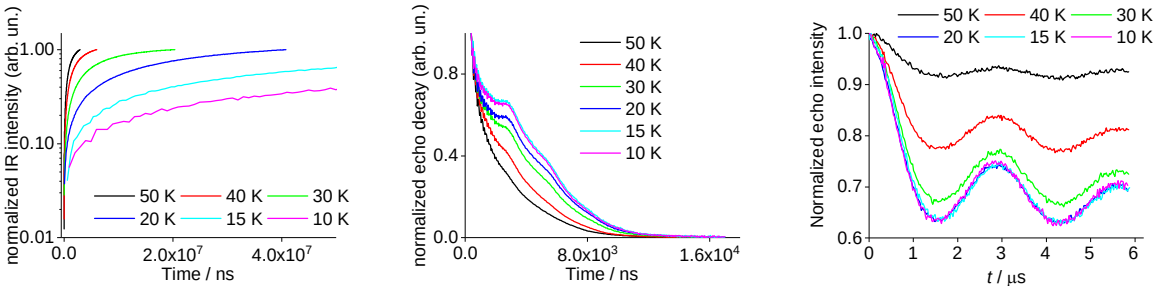

Fig. S5. T_1 and T_m measurements of the nitroxide spin labels (left and middle, respectively) and nitroxide-nitroxide distance measurements between 50 K and 10 K measured at Q-band frequencies on the Co^{II}/L = 0.5 complex.

The nitroxide-nitroxide PELDOR distance measurements on the Co^{II} series measured at X-band at 10 K are shown in Fig. S6.

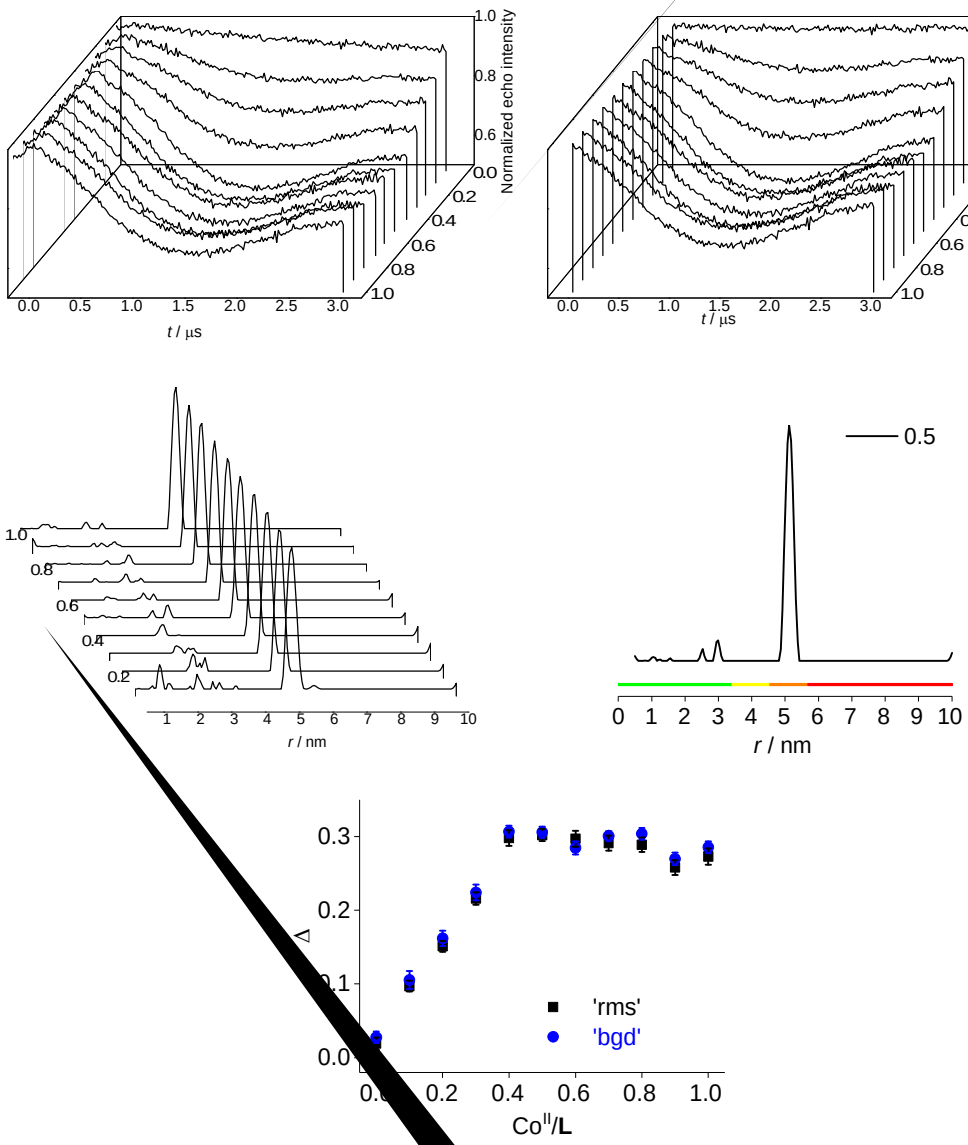

Fig. S6. Co^{II} 'pseudo-titration' series measured with PELDOR at X-band. Background uncorrected (top left), background corrected (top right) PELDOR data, distance distributions (middle left) and distance distribution of the Co^{II}/L = 0.5 ratio including colour coded reliability bars (middle right) and modulation depth Δ *vs* Co^{II}/L as derived from the fit of the trace ('rms', black points, bottom) and upon variation of the background for densities between half and double that of the 0.0 ratio ('bgd', blue points, bottom).

5. Cu^{II} 'pseudo-titration' series

In order to assess the optimum experimental temperature for performing PELDOR on the Cu^{II} series, we measured the longitudinal and transverse relaxation times (T_1 and T_m, respectively) of the nitroxide spins as well as the modulation depth of the nitroxide-nitroxide PELDOR experiment over a range of temperatures of the Cu^{II}/**L** = 0.4 complex at Q-band frequencies (Fig. S7).

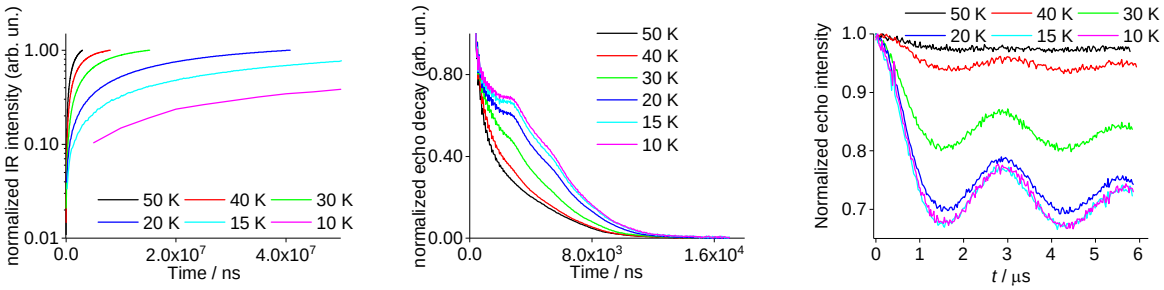

Fig. S7. T_1 and T_m measurements of the nitroxide spin labels (left and middle, respectively) and nitroxide-nitroxide distance measurements between 50 K and 10 K measured at Q-band frequencies on the Cu^{II}/L = 0.5 complex.

The nitroxide-nitroxide PELDOR distance measurements on the Cu^{II} series measured at X-band at 10 K are shown in Fig. S8.

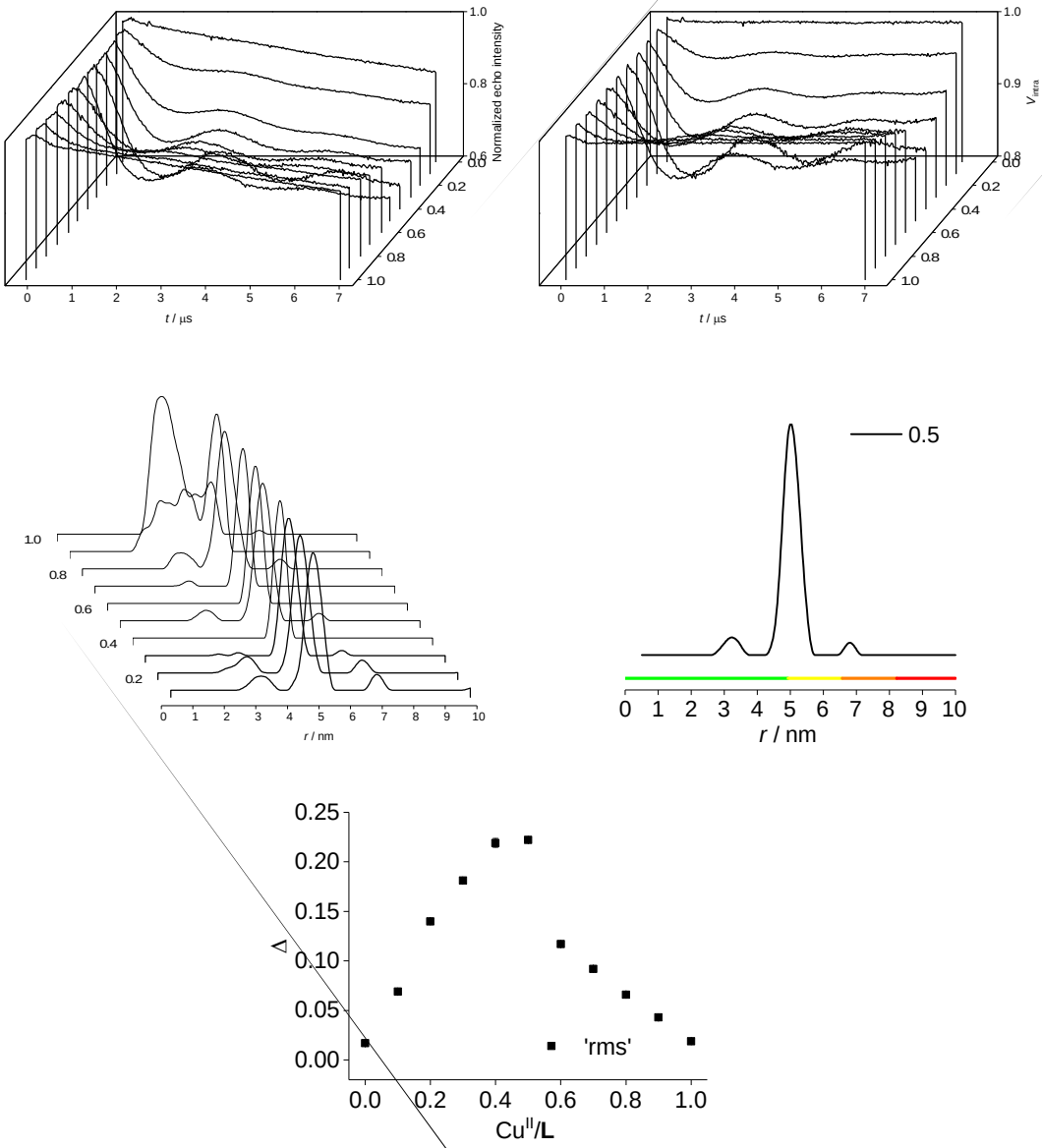

Fig. S8. Cu^{II} 'pseudo-titration' series measured with PELDOR at Q-band. Background uncorrected (top left), background corrected (top right) PELDOR data, distance distributions (middle left) and distance distribution of the Cu^{II}/L = 0.5 ratio including colour coded reliability bars (middle right) and modulation depth Δ *vs* Cu^{II}/L as derived from the fit of the trace ('rms', black points, bottom).

6. Modelled M^{II}-nitroxide modulation depths

To estimate the sensitivity of M^{II}-nitroxide PELDOR modulation depths for identifying binding cooperativities, we simulated the respective modulation depths as a function of **L**/M^{II} ratio (note that this is inverse to all other experiments in this work) based on the assumption that paramagnetic ions not bound to **L** do not exhibit any modulation depth (*e.g.* **L**/M^{II} = 0), complexes bound to a single **L** (*e.g.* **L**/M^{II} = 1, anti-cooperatively) will have $\Delta = \lambda$ and complexes binding two **L** (*e.g.* **L**/M^{II} = 2) will have $\Delta = 2\lambda - \lambda^2$. From **L**/$M^{II}$ and the cooperativity the populations of the different species can be calculated and the overall modulation depth is given by the weighted sum over all three species (Fig. S9). In practice, for **L**/M^{II} from 0 to 2 there is excess M^{II} that can either lead to solvated M^{II} ($\Delta_M = 0$) and bis-complex with two **L** bound ($\Delta_{ML2} = 2\lambda - \lambda^2$) or double the amount of complex with a single **L** bound ($\Delta_{ML} = \lambda$). The difference between Δ_{ML2} and Δ_{ML} is just $-\lambda^2$ and will be small for λ achievable with rectangular pulses ($\lambda = 0.4$ simulated below).

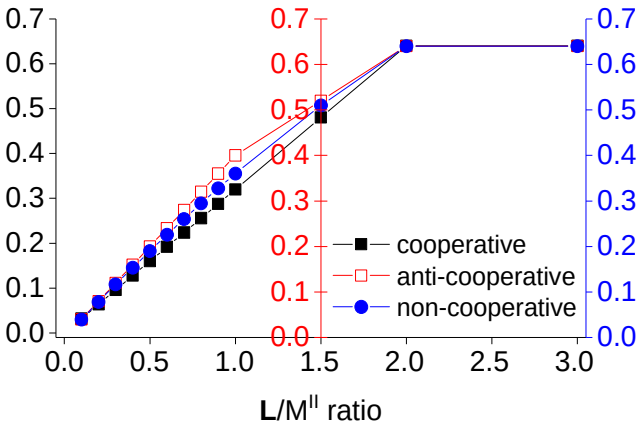

Fig. S9. Modelled Δ vs L/M^{II} in metal-nitroxide distance measurements where the metal amount is kept constant while increasing the amount of added L.

7. Details on WURST pulses

The broadband experiments were performed using a WURST inversion pulse at ω_B.[6, 7] The pulse length used was 80 ns using maximum microwave field strength of 17.14 G, a sweep rate of 5 MHz/ns and truncation parameter of 7. The WURST pulse shape and excitation profile are shown in Fig. S10.

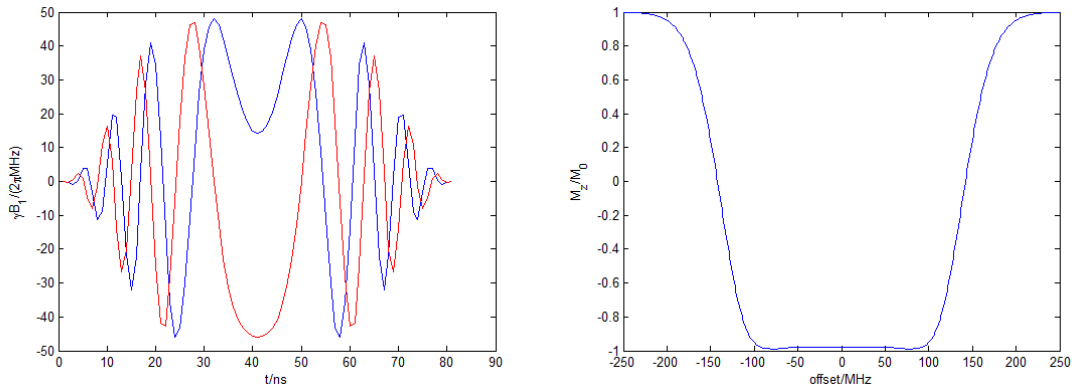

Fig. S10. The time domain shape of the WURST pulse with the *x*, *y* components shown in red and blue, respectively (left) and excitation bandwidth profile of the WURST inversion pulse (right).

8. Co^{II}-nitroxide distance measurements

Broadband (WURST) inversion pulse

The Co^{II}-nitroxide distances of the Co^{II}/**L** ratios 0.5 and 1.0 were measured with WURST inversion pulse[6, 7] at X-band frequencies and are shown in Fig. S11.

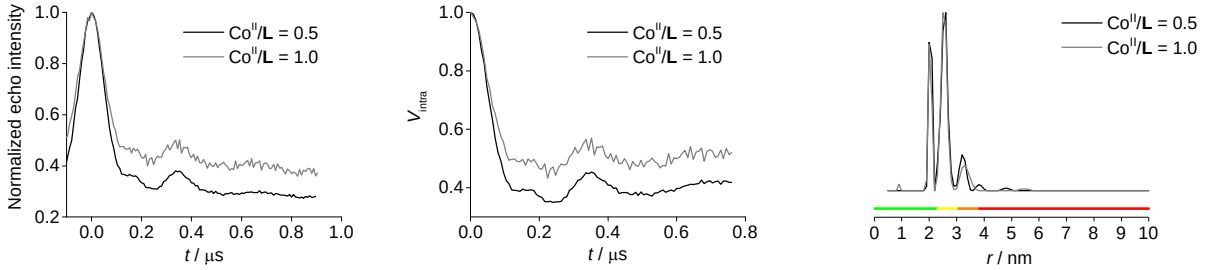

Fig. S11. Cobalt-nitroxide PELDOR distance measurements with WURST inversion pulse measured at X-band frequencies on Co^{II}/L ratios 0.5 and 1.0. Background uncorrected (left), background corrected (middle) PELDOR data and distance distributions including colour coded reliability bars (right).

The Co^{II}-nitroxide distances with confidence intervals (validated) of the broadband measurements of the 0.5 and 1.0 Co^{II}/**L** ratios are shown in Fig. S12.

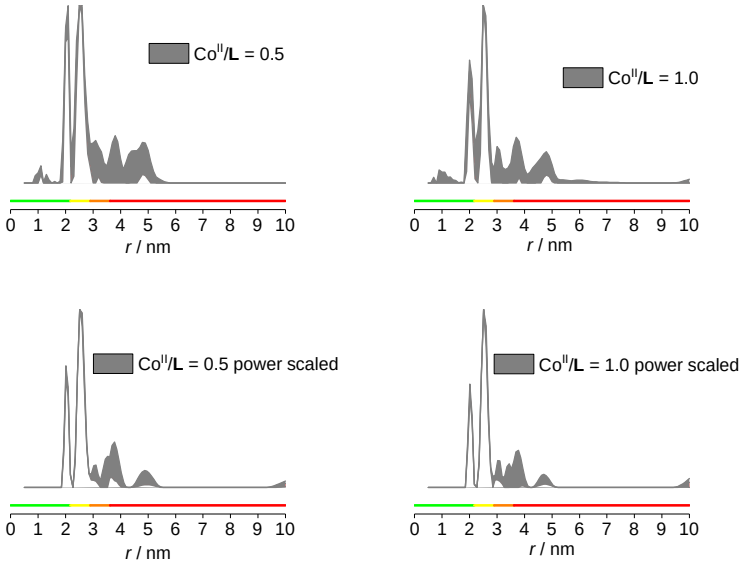

Fig. S12. Cobalt-nitroxide distance distributions including confidence intervals of the 0.5 (left) and 1.0 Co^{II}/L (right) complexes measured with broadband PELDOR at X-band before (top) and after (bottom) 'power-scaling'.

Rectangular inversion pulse

The Co^{II}-nitroxide distance of the Co^{II}/**L** = 0.5 complex was measured with rectangular inversion pulse at X-band frequencies and is shown in Fig. S13.

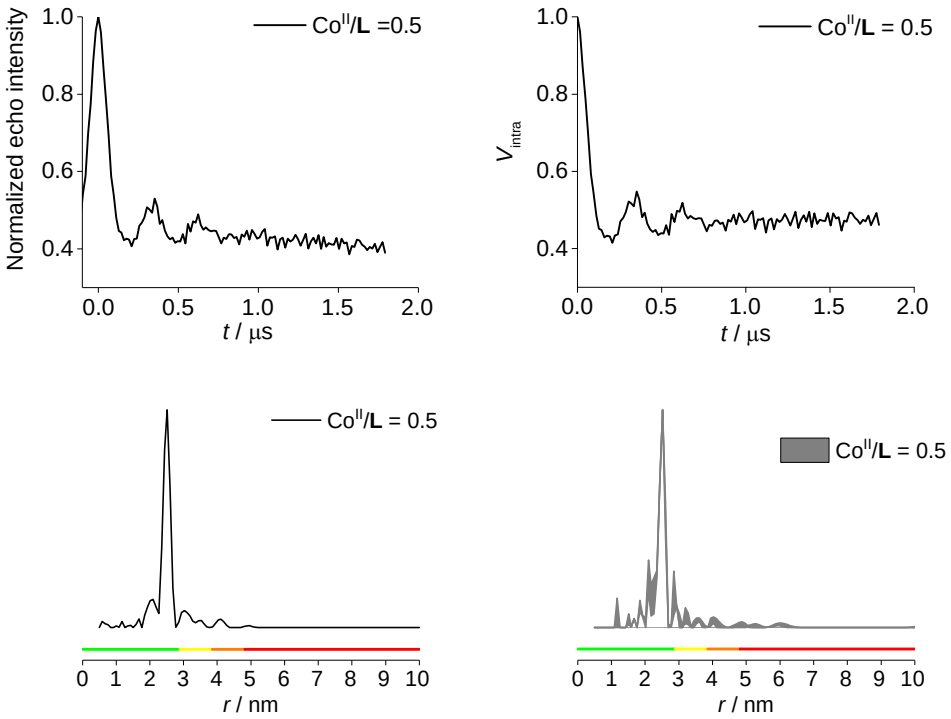

Fig. S13. Background uncorrected (top left), background corrected (top right) PELDOR data and distance distribution without and with confidence intervals (bottom left and right, respectively) of complex Co^{II}/L = 0.5 measured at X-band frequencies with rectangular inversion pulse.

9. Cu^{II}-nitroxide distance measurements

Broadband (WURST) inversion pulse

The Cu^{II}-nitroxide distances of the Cu^{II}/**L** ratios 0.5 and 1.0 were measured with WURST inversion pulse[6, 7] at X-band frequencies and are shown in Fig. S14. The distance distribution of the 0.5 Cu^{II}/**L** ratio was generated without applying any background removal. Removal of the intermolecular interactions was unfeasible here due to the large modulation depth of this measurement that reaches 100%.

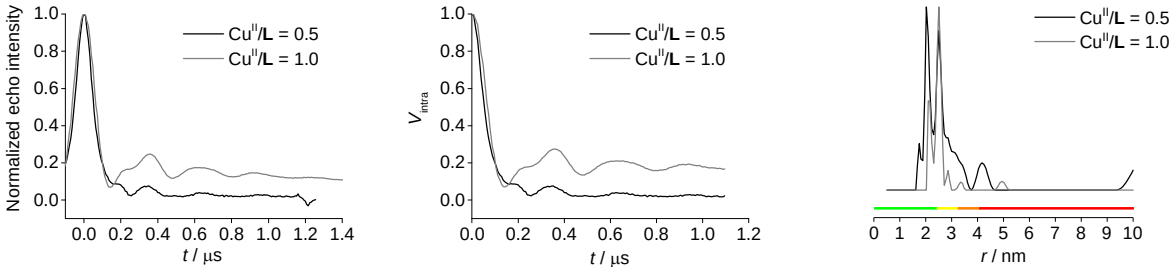

Fig. S14. Copper-nitroxide PELDOR distance measurements with WURST inversion pulse measured at X-band frequencies on Cu^{II}/L ratios 0.5 and 1.0. Background uncorrected (left), background corrected (middle) PELDOR data and distance distributions including colour coded reliability bars (right).

The Cu^{II}-nitroxide distance with confidence intervals (validated) of the broadband measurement of the 1.0 Cu^{II}/**L** ratio is shown in Fig. S15 (top, right). The validated distance distribution of the 0.5 Cu^{II}/**L** ratio could not be generated due to not being able to remove the background contributions in the primary data. Additionally, the data were post-processed employing 'power-scaling'. The 'power-scaled' data of 0.5 Cu^{II}/**L** ratio yielded again a PELDOR trace with virtually 100% modulation depth that could not be subjected to validation of the background removal.

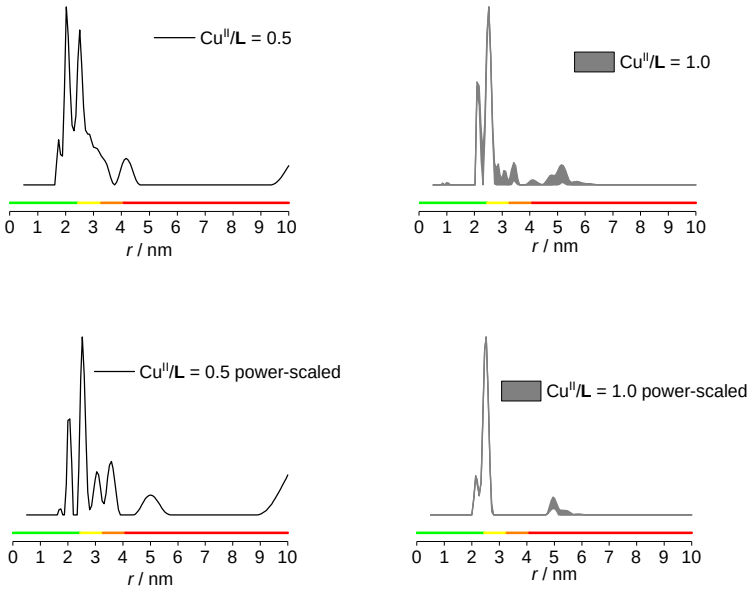

Fig. S15. Copper-nitroxide distance distribution of the 0.5 Cu^{II}/L ratio without confidence intervals before (top left) and after (bottom left) power 'scaling' and of the 1.0 Cu^{II}/L ratio including confidence intervals before (top right) and after (bottom right) 'power-scaling' measured with broadband PELDOR at X-band.

Rectangular inversion pulse

The Cu^{II}-nitroxide distance of the Cu^{II}/**L** = 0.5 was measured with rectangular inversion pulse at X-band frequencies and is shown in Fig. S16.

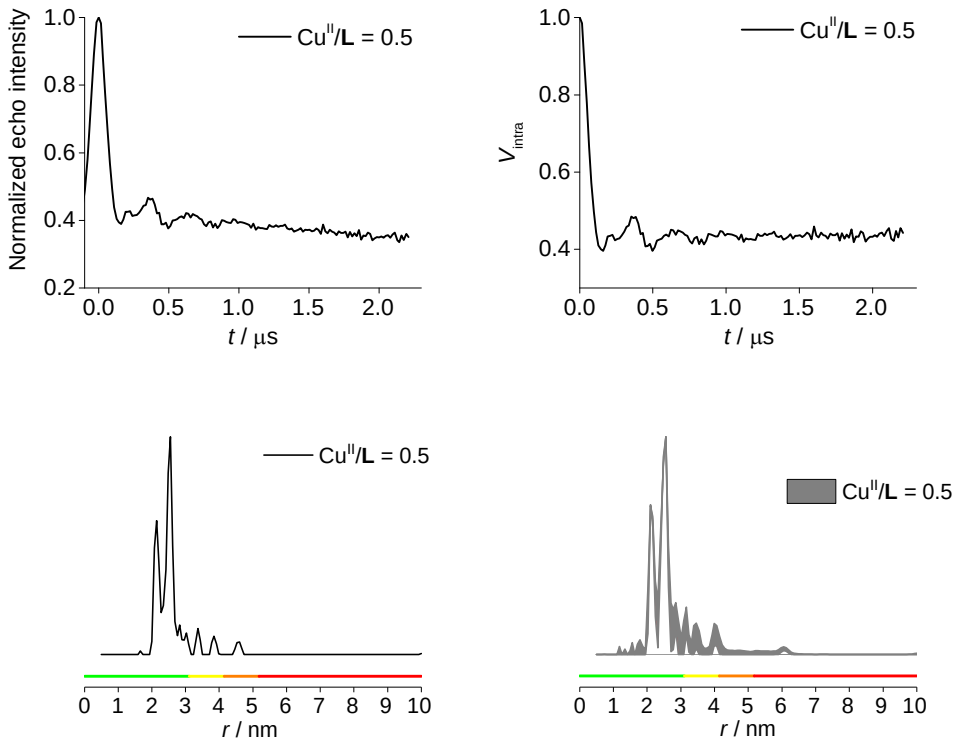

Fig. S16. Background uncorrected (top left), background corrected (top right) PELDOR data and distance distribution without and with confidence intervals (bottom left and right, respectively) of ratio Cu^{II}/L = 0.5 measured at X-band frequencies with rectangular inversion pulse.

10. Synthesis and characterization of ligand K

Ligand **K** was synthesized in an analogous procedure to the synthesis of **L**,[8] i.e. *via* an esterification of 4-iodophenol with 2,2,5,5-tetramethyl-pyrroline-*N*-oxyl-3-carboxylic acid (TPC) followed by a Sonogashira cross-coupling between the esterification product (4-iodophenyl 1-oxyl-2,2,5,5-tetramethyl-2,5-dihydro-1*H*-pyrrole-3-carboxylate) and a terpyridine-based ligand[9] (4'-(4-ethynylphenyl)-2,2':6',2''-terpyridine) bearing a terminal acetylene (Scheme S1).

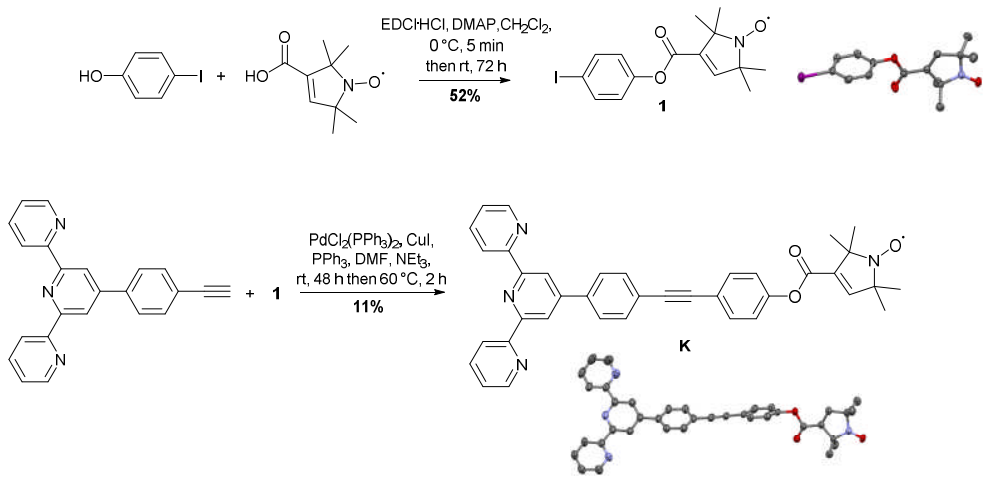

Scheme S2. Synthesis of ligand K.

<u>Synthesis and characterization of 4-iodophenyl 1-oxyl-2,2,5,5-tetramethyl-2,5-dihydro-1*H*-pyrrole-3-carboxylate (1)</u>

4-Hydroxy-4'-iodobiphenyl (0.51 g, 2.32 mmol, 1.0 equiv.), DMAP (0.03 g, 0.24 mmol, 10 mol%) and EDCI·HCl (0.51 g, 2.64 mmol, 1.1 equiv.) were added to a solution of 1-oxyl-2,2,5,5-tetramethyl-pyrrolin-3-carboxylic acid (TPC) (0.44 g, 2.39 mmol, 1.0 equiv.) in CH_2Cl_2 (20 mL) at 0 °C. The reaction mixture was stirred at 0 °C for 5 min, warmed to rt and stirred in the dark for 72 h. The solvent was removed *in vacuo*, the residue was taken up in CH_2Cl_2 (20 mL), washed with saturated $NaHCO_3$ (2 × 20 mL) and H_2O (2 × 20 mL) before drying over Na_2SO_4. The layers were separated and removal of the solvent *in vacuo* afforded the crude product, which was purified by recrystallization from hexane/CH_2Cl_2 (1/1) at 0 °C to give the title compound **1** (0.46 g, 1.2 mmol, 52%) as intense yellow crystals. The crystals were suitable for x-ray diffraction. mp 138.4-139.3 °C; ν_{max} (cm^{-1}) 1151, 1193, 1342, 1479,1625, 1728; *m/z* (APCI$^+$) 387 ([*M* + H]$^+$, 100%); HRMS (APCI$^+$) $C_{15}H_{18}INO_3$ ([*M* + H]$^+$), found 387.0322, calculated 387.0326 (− 1.0 ppm). $C_{15}H_{17}INO_3$ calculated C, 46.65; H, 4.44; N, 3.63; found C, 46.55; H, 4.54; N, 3.69%. Crystal data. $C_{15}H_{17}INO_3$, *M* = 386.21, triclinic, *a* = 9.0407(16), *b* = 9.359(2), *c* = 10.1910(19) Å, *α* = 105.821(3), *β* = 94.648(3), *γ* = 105.915(4) °, *U* = 786.4(3) Å^3, *T* = 173 K, space

group $P\bar{1}$ (no. 2), Z = 2, 9770 reflections measured, 2873 unique (R_{int} = 0.0493), which were used in all calculations. The final R_1 [$I > 2\sigma(I)$] was 0.0234 and wR_2 (all data) was 0.0563.

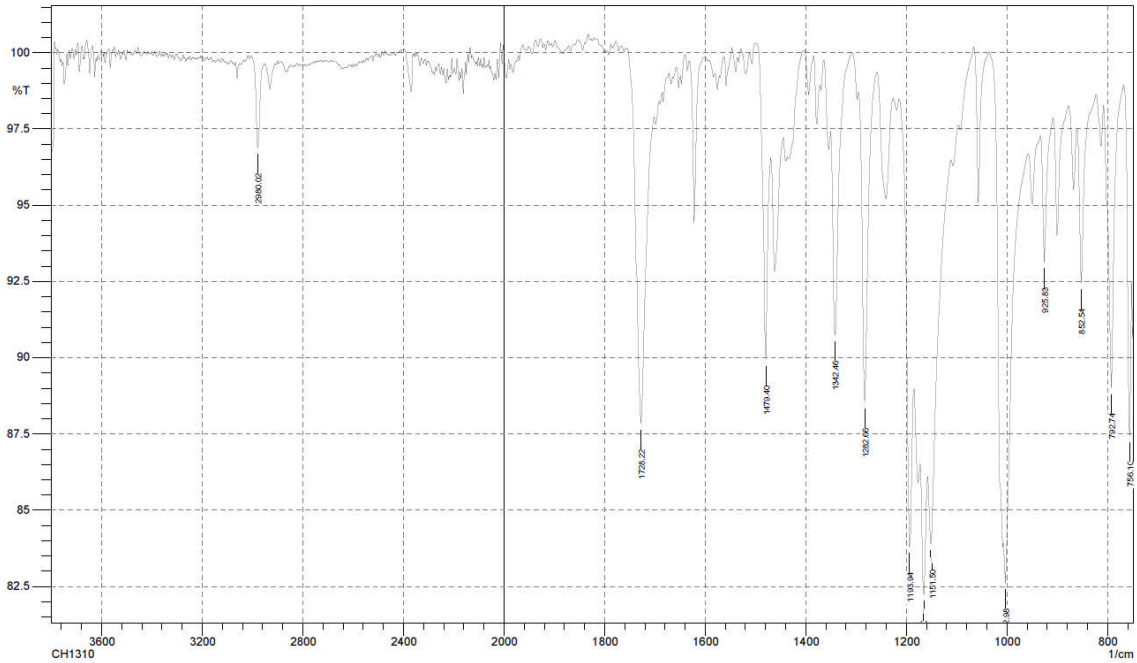

Fig. S17. IR spectrum of 1.

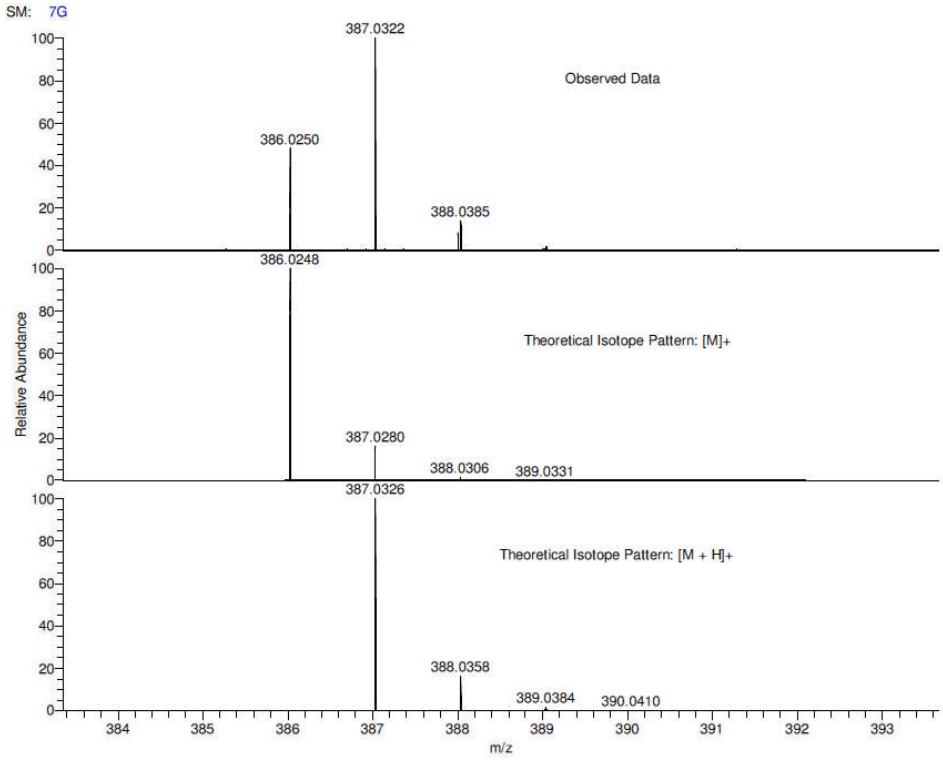

Fig. S18. Mass spectrum of 1.

Synthesis and characterization of 4-((4-([2,2':6',2''-terpyridin]-4'-yl)phenyl)ethynyl)phenyl 1-oxyl-2,2,5,5-tetramethyl-2,5-dihydro-1*H*-pyrrole-3-carboxylate (K)

4-Iodophenyl 1-oxyl-2,2,5,5-tetramethyl-2,5-dihydro-1*H*-pyrrole-3-carboxylate **1** (0.40 g, 1.0 mmol, 1.0 equiv.) was added to a Schlenk flask containing NEt_3 (80 mL) and anhydrous DMF (18 mL) and $PdCl_2(PPh_3)_2$ (0.12 g, 0.17 mmol, 17 mol%). The resulting solution was degassed by freeze-pump-thaw cycles (× 4). 4'-(4-ethynylphenyl)-2,2':6',2''-terpyridine (0.41 g, 1.24 mmol, 1.2 equiv.) and PPh_3 (0.13 g, 0.50 mmol) were added to a separate Schlenk flask containing NEt_3 (40 mL) and anhydrous DMF (10 mL). The resulting mixture was degassed by freeze-pump-thaw cycles (× 4). CuI (0.13 g, 0.68 mmol, 68 mol%) was added to the first flask followed by dropwise addition of the first solution to the second solution over the course of 15 minutes. The resulting orange solution was stirred at rt for 48 h, then heated to 60 °C for 2 h. After cooling to rt the solvents were removed *in vacuo*, the residue was re-dissolved in CH_2Cl_2 (100 mL) and washed with H_2O (3 × 100 mL) and brine (2 × 100 mL). The organic phase was dried over Na_2SO_4 and concentrated *in vacuo* to afford the crude product. Flash chromatography on alumina (4% H_2O, 9.5/0.5 to 5.0/5.0 petrol/EtOAc, then 9/1 DCM/MeOH) afforded the title compound (0.068 g, 0.11 mmol, 11%) as a yellow powder. Crystals suitable for x-ray diffraction were obtained from hexane/CH_2Cl_2 mixture (1/1) at 0 °C. mp 198.1-199.8 °C; ν_{max} (cm^{-1}) 1163, 1195, 1350, 1386, 1516, 1583, 1734, 2150, 2976, 3075; *m*/*z* ($APCI^+$) 592 ($[M + H]^+$, 100%); HRMS ($APCI^+$) $C_{41}H_{34}N_4O_3$ ($[M + H]^+$), found 592.2469, calculated 592.2469 (0.0 ppm); $C_{38}H_{31}N_4O_3$ calculated C, 77.14; H, 5.28; N, 9.47%; found C, 77.02; H, 5.39; N, 9.40%. Crystal data. $C_{40}H_{35}Cl_4N_4O_3$, M = 761.55, monoclinic, a = 16.901(3), b = 9.2057(13), c = 47.963(8) Å, β = 91.149(6) °, U = 7461(2) $Å^3$, T = 173 K, space group $I2/a$ (no. 15), Z = 8, 58867 reflections measured, 6853 unique (R_{int} = 0.1102), which were used in all calculations. The final R_1 [$I > 2\sigma(I)$] was 0.1008 and wR_2 (all data) was 0.3125.

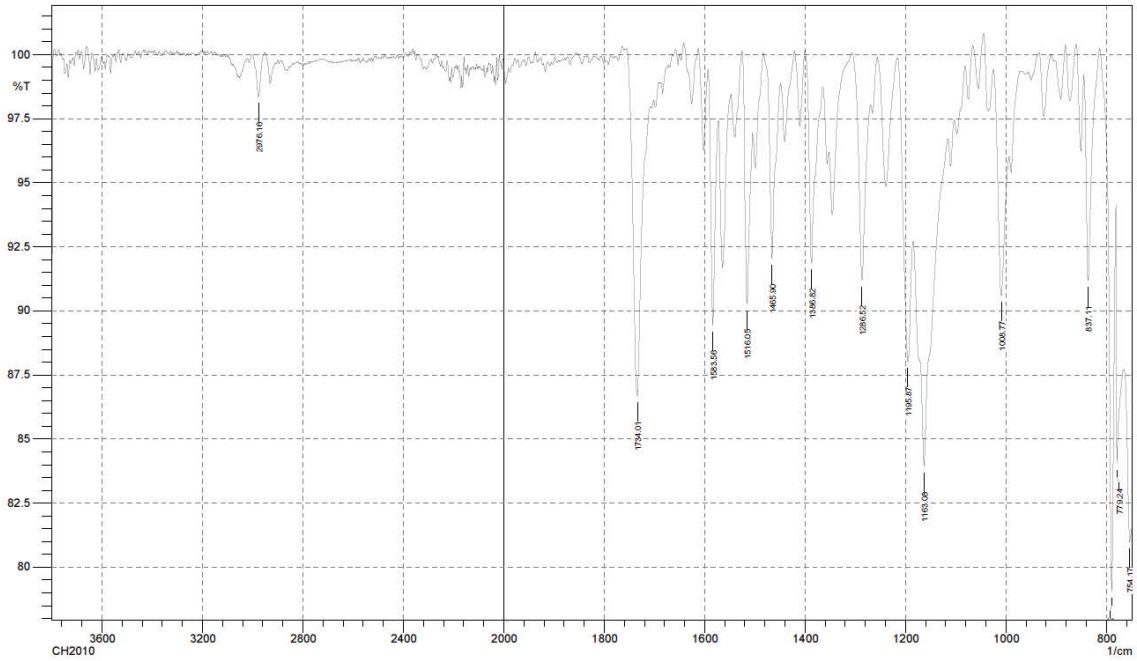

Fig. S19. IR spectrum of K.

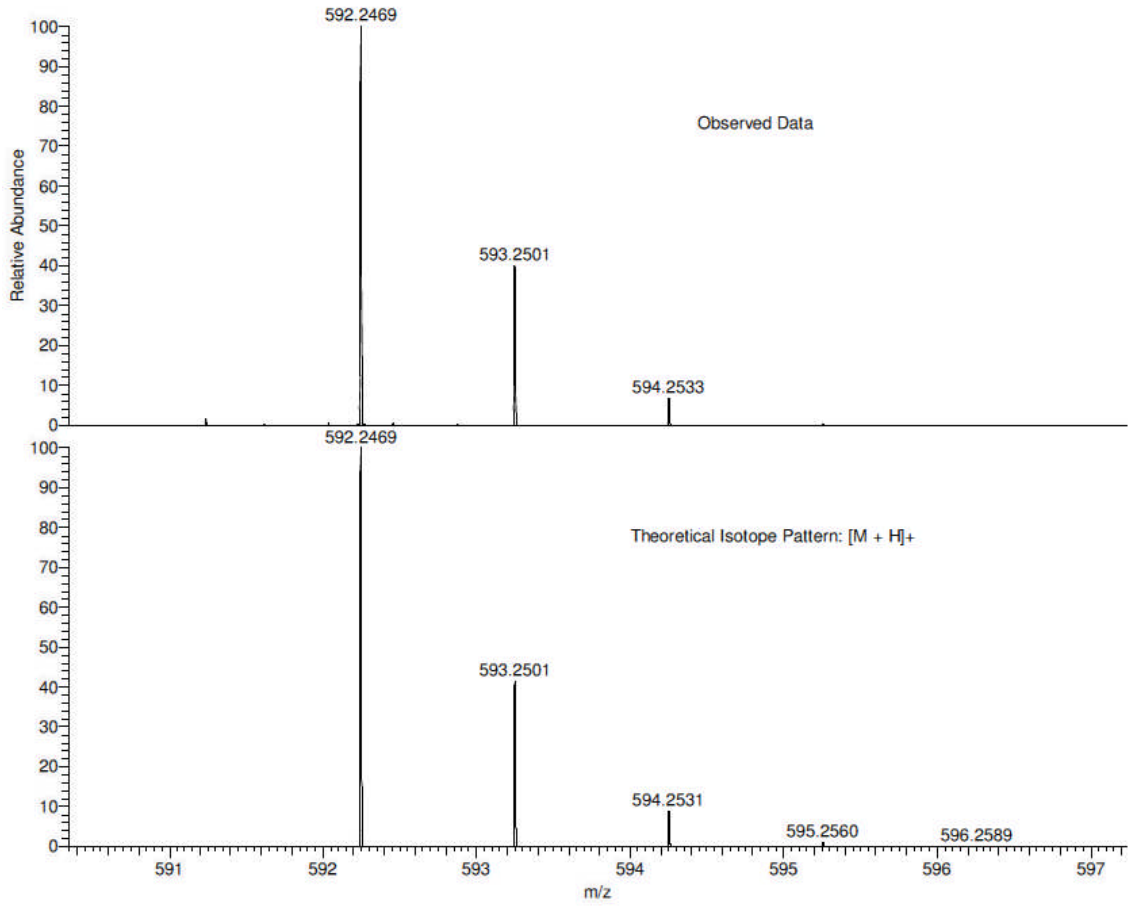

Fig. S20. Mass spectrum of K.

11.Ligand exchange ('scrambling') mixtures

The nitroxide-nitroxide PELDOR distance measurements of the mixtures of the bis-complexes with ligands **K**, **L** measured with rectangular inversion pulse at Q-band frequencies are shown in Fig. S21.

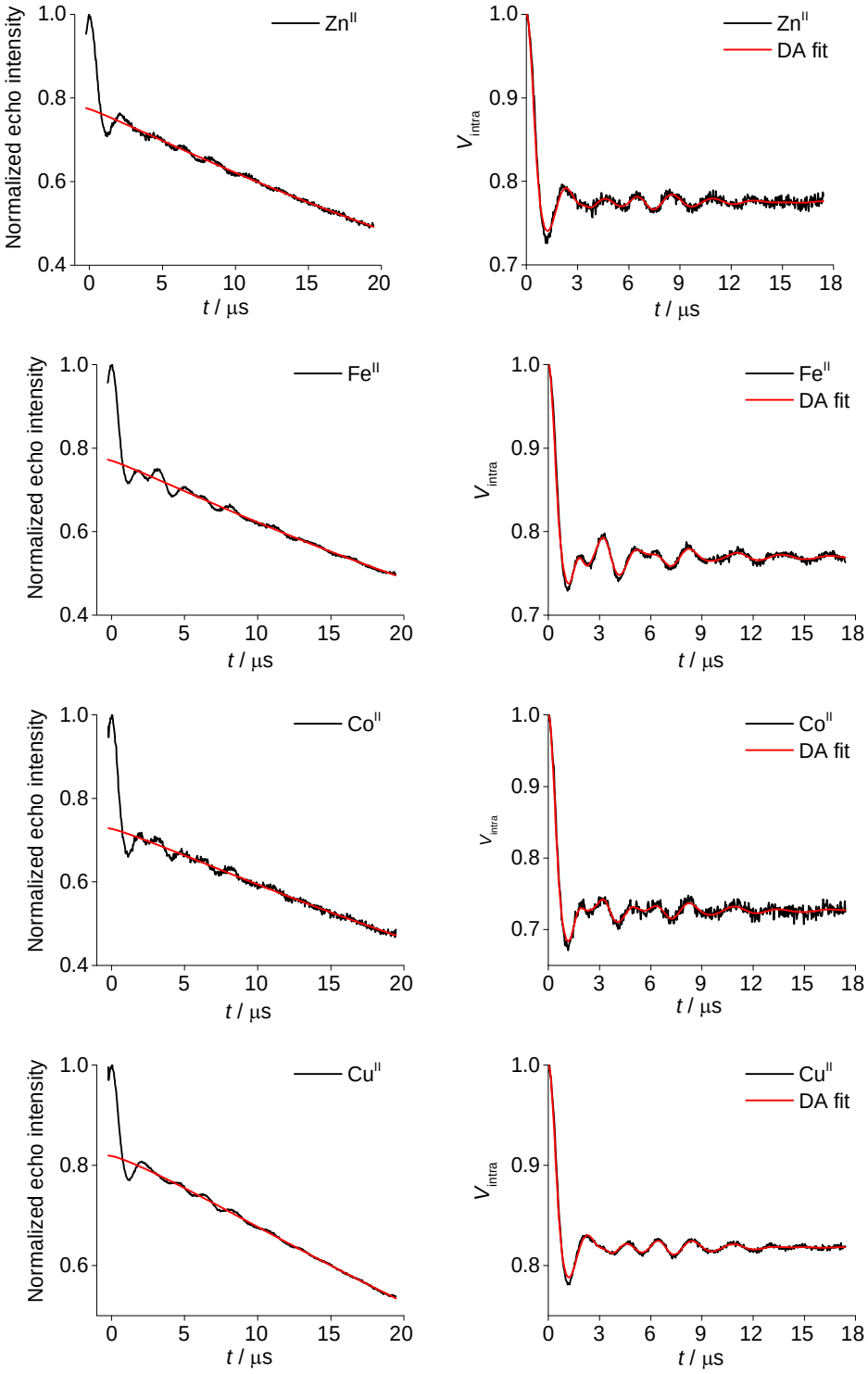

Fig. S21. Background uncorrected (left, raw data in black, background fit in red) and background corrected (right, data in black simulation based on extracted distance distribution in red) PELDOR data on the mixture of the bis-complexes of Zn^{II}, Fe^{II}, Co^{II} and Cu^{II} (from top to bottom) with ligands K and L measured at Q-band frequencies with a rectangular inversion pulse.

The nitroxide-nitroxide distances with confidence intervals (validated) of the mixtures of the bis-complexes of all metals with ligands **K** and **L** measured at Q-band frequencies with rectangular inversion pulse are shown in Fig. S22.

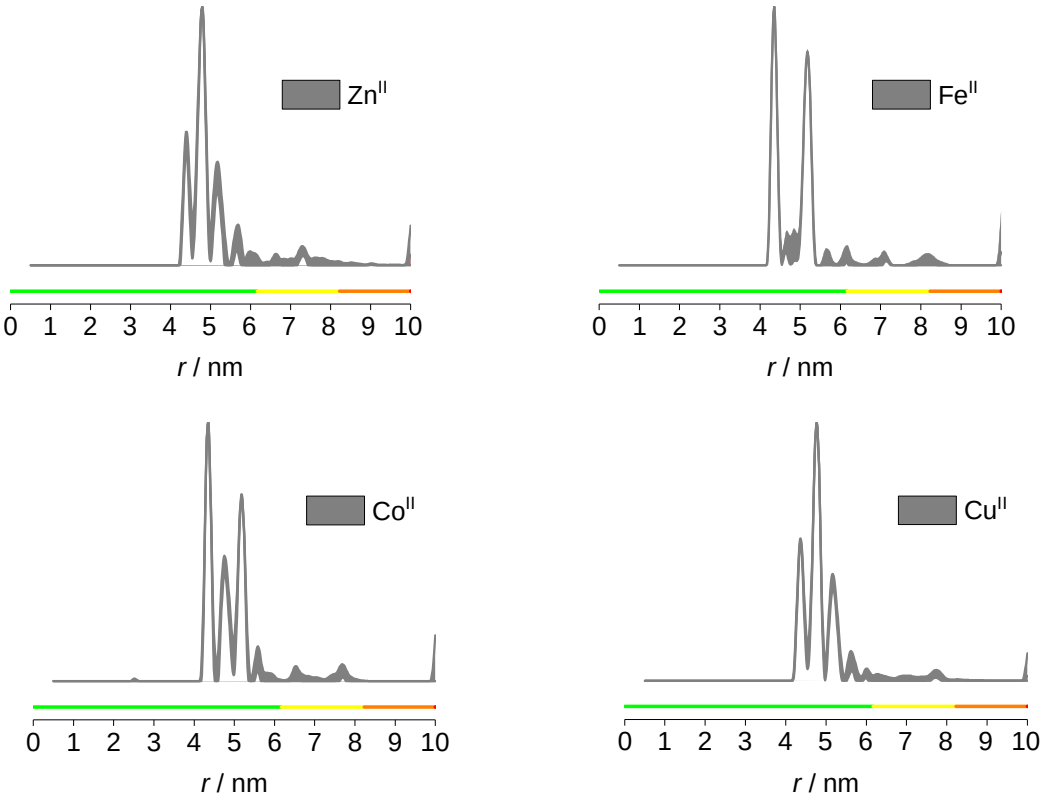

Fig. S22. Distance distributions including confidence intervals and colour coded reliability bars of the nitroxide-nitroxide PELDOR on mixtures of the bis-complexes of Zn^{II} (top left), Fe^{II} (top right), Co^{II} (bottom left) and Cu^{II} (bottom right) with ligands K and L measured at Q-band frequencies with rectangular inversion pulse.

12. References

1. *CrystalClear-SM Expert v. 2.1; Rigaku Americas, Rigaku Americas, The Woodlands, Texas, USA and Rigaku Corporation, Tokyo, Japan 2015*.
2. *DIRDIF-99. Beurskens, P. T.; Beurskens, G.; de Gelder, R.; Garcia-Granda, S.; Gould, R. O.; Israel, R.; Smits, J. M. M. Crystallography Laboratory, University of Nijmegen, The Netherlands, 1999*.
3. M. C. Burla, R. Caliandro, M. Camalli, B. Carrozzini, G. L. Cascarano, C. Giacovazzo, M. Mallamo, A. Mazzone, G. Polidori and R. Spagna, *J. Appl. Crystallogr.*, 2012, **45**, 357-361.
4. G. M. Sheldrick, *Acta Crystallogr. C Struct. Chem.*, 2015, **71**, 3-8.
5. *CrystalStructure v4.2. Rigaku Americas, The Woodlands, Texas, USA, and Rigaku Corporation, Tokyo, Japan, 2015.*
6. P. E. Spindler, S. J. Glaser, T. E. Skinner and T. F. Prisner, *Angew. Chem. Int. Ed. Engl.*, 2013, **52**, 3425-3429.
7. E. Kupce and R. Freeman, *J. Magn. Reson., Ser A* 1995, **115**, 273-276.
8. K. Ackermann, A. Giannoulis, D. B. Cordes, A. M. Z. Slawin and B. E. Bode, *Chem. Commun.*, 2015, **51**, 5257-5260.
9. V. Grosshenny, F. M. Romero and R. Ziessel, *J. Org. Chem.*, 1997, **62**, 1491-1500.